A Water-Stable Luminescent Zn-MOF Based on a Conjugated π-electron Ligand as an Efficient Sensor for Atorvastatin and Its Application in Pharmaceutical Samples

Luis D. Rosales-Vázquez,[a] Josue Valdes-García,[a] J. M. Germán-Acacio,[b] José C. Páez-Franco,[b] Diego Martínez-Otero,[c] Alfredo R. Vilchis-Néstor, Joaquín Barroso-Flores,[c] Víctor Sánchez-Mendieta[c] and Alejandro Dorazco-González[a*]

[a]Instituto de Química, Universidad Nacional Autónoma de México. Circuito Exterior, Ciudad Universitaria, Ciudad de México, 04510, México. E-mail: adg@unam.mx
[b]Red de Apoyo a la Investigación, Instituto Nacional de Ciencias Médicas y Nutrición SZ-Universidad Nacional Autónoma de México (CIC-UNAM)
[c]Centro Conjunto de Investigación en Química Sustentable UAEM-UNAM, Carretera Toluca-Ixtlahuaca Km. 14.5, San Cayetano, Toluca, Estado de México, 50200, México. E-mail: vsanchezm@uaemex.mx

Electronic Supplementary Information

General considerations

Materials and methods

All chemicals are commercially available ([1,1′:4′,1″]Terphenyl- 3,3″,5,5″-tetracarboxylic acid 95%; $Zn(CF_3SO_3)_2$ 98%; atorvastatin calcium trihydrate 98%; rosuvastatin calcium 98%; pravastatin sodium salt hydrate 98%; fluvastatin sodium hydrate 98%; *N,N*-dimethylformamide 99% and ethanol anhydrous 98% from Sigma-Aldrich (St. Louis, Missouri, United States)) were used as received.

The FT-IR spectrum was recorded in the range of 4000–600 cm^{-1} by using the standard Pike ATR cell on a Bruker Tensor 27 FT-IR spectrophotometer (Bruker Optik GmbH, Ettlingen, Germany). Elemental analysis for C, H, and N were carried out by standard methods using a Vario Micro-Cube analyzer.

Powder X-ray diffraction (PXRD) was conducted using a Bruker D8 ADVANCE X-ray powder diffractometer (Cu-Kα, λ= 1.5418 Å) (Bruker AXS GmbH, Karlsruhe, Germany) with the 2θ range of 5–50◦.

Thermogravimetric analyses were performed using TA Instruments equipment, under a dinitrogen atmosphere, at a heating rate of 10 ◦C min^{-1}, and from 25 to 450 ◦C.

Scanning electron microscopy (SEM) analysis were carried out using a JSM-6510LV microscope from JEOL (JEOL, Ltd, Akishima, Tokyo, Japan) equipped with a Bruker QUANTAX 200 energy-dispersive X-ray spectrometer (EDS) (Bruker Nano GmbH, Adlershof. Berlin, Germany) for elemental characterization. The crystals were dried at room-temperature conditions and fixed on Al stubs with carbon double tape and finally coated with a thin layer of gold using a Denton IV sputtering chamber before SEM imaging acquisition.

^{13}C CPMAS NMR experiment was recorded with a Bruker Avance II 300 spectrometer (operating at: ^{1}H 300 MHz and ^{13}C 75 MHz). *ss* NMR measurement was carried out on a 4 mm rotor double resonance and recorded with a contact time of 3 ms and a delay of 10 s at 8 kHz spinning rate at ambient temperature.

Liquid chromatographic determination of atorvastatin: From the extracted tablet stock solution, a dilution 1/400 was performed in ethanol, and an aliquot of 40 µL was injected into an HPLC 1260 Infinity II (Agilent) coupled to a diode array detector. The UV detection was set to 220 nm. The mobile phase was 0.01 mol/L sodium dihydrogen phosphate pH 5.5 in distilled water and 40% ethanol (Sigma-HPLC grade) with a constant rate flow of 2 ml min^{-1}. The analysis was performed on a column Zorbax Eclipse XDB-C18 (Agilent) equilibrated at 37 °C. To calculate the final concentration of the sample extracted, a linear analytical curve (0 – 88 µM mL^{1}) was prepared with pure atorvastatin (PHR1422-Sigma). The corresponding peak for atorvastatin is 2.55 min.

Table S1. Crystal data and structural refinement parameters for Zn-MOF, **1**.

Empirical formula	$C_{50.21}H_{43.23}O_{20.41}Zn_3$
Formula weight	1002.72
Temperature (K)	100(2)
Wavelength (Å)	1.54178
Crystal system	Monoclinic
Space group	*C2/c*
a (Å)	10.1439(6)
b (Å)	28.6171(15)
c (Å)	18.2650(10)
α (°)	90
β (°)	90.938(3)
γ (°)	90
Volume ($Å^3$)	5301.4(5)
Z	4
D_{calc} (Mg/m^3)	1.256
Absorption coefficient (mm^{-1})	2.090
F(000)	2016
Crystal size (mm^3)	0.172 x 0.098 x 0.059
Theta range for data collection (°)	3.088 to 69.123
Index ranges	-12<=h<=12, 0<=k<=34, 0<=l<=22
Reflections collected	4849
Independent reflections	4849 [R(int) = 0.0225]
Refinement method	Full-matrix least-squares on F^2
Data/restraints/parameters	4849 / 398 / 346
Goodness-of-fit on F^2	1.120
Final R indices [I>2sigma(I)]	R1 = 0.0749, wR2 = 0.2167
R indices (all data)	R1 = 0.0815, wR2 = 0.2230
Largest diff. peak and hole ($e.Å^{-3}$)	0.830 and -0.951

Table S2. Selected bond distances (Å) and angles (˚) for **1**.

Bond lengths (Å)			
Zn(1)-O(1)	2.012(4)	Zn(2)-O(7)	2.000(5)
Zn(1)-O(1)#1	2.012(4)	Zn(2)-O(2)#6	2.008(4)
Zn(1)-O(6)#2	2.085(4)	Zn(2)-O(5)#7	2.013(4)
Zn(1)-O(6)#3	2.085(4)	Zn(2)-O(4)#8	2.038(4)
Zn(1)-O(4)#4	2.171(4)	Zn(2)-O(8)	2.425(6)
Zn(1)-O(4)#5	2.171(4)	Zn(2)-O(7)	2.000(5)

Angles (˚)			
O(1)-Zn(1)-O(1)#1	180.0	O(6)#2-Zn(1)-O(4)#5	91.40(16)
O(1)-Zn(1)-O(6)#2	95.51(17)	O(6)#3-Zn(1)-O(4)#5	88.60(16)
O(1)#1-Zn(1)-O(6)#2	84.49(17)	O(4)#4-Zn(1)-O(4)#5	180.0(2)
O(1)-Zn(1)-O(6)#3	84.49(17)	O(7)-Zn(2)-O(2)#6	105.40(19)
O(1)#1-Zn(1)-O(6)#3	95.51(17)	O(7)-Zn(2)-O(5)#7	97.75(19)
O(6)#2-Zn(1)-O(6)#3	180.0(2)	O(2)#6-Zn(2)-O(5)#7	102.20(19)
O(1)-Zn(1)-O(4)#4	88.60(16)	O(7)-Zn(2)-O(4)#8	132.85(19)
O(1)#1-Zn(1)-O(4)#4	91.40(16)	O(2)#6-Zn(2)-O(4)#8	107.50(16)
O(6)#2-Zn(1)-O(4)#4	88.60(16)	O(5)#7-Zn(2)-O(4)#8	107.11(17)
O(6)#3-Zn(1)-O(4)#4	91.40(16)	O(7)-Zn(2)-O(8)	57.71(19)
O(1)-Zn(1)-O(4)#5	91.40(16)	O(2)#6-Zn(2)-O(8)	91.9(2)
O(1)#1-Zn(1)-O(4)#5	88.60(16)	O(5)#7-Zn(2)-O(8)	154.54(18)
		O(4)#8-Zn(2)-O(8)	88.29(2)

Symmetry transformations used to generate equivalent atoms:

#1 -x+1,-y+1,-z #2 x-1/2,-y+1/2,z-1/2 #3 -x+3/2,y+1/2,-z+1/2
#4 -x+1,y,-z+1/2 #5 x,-y+1,z-1/2 #6 x-1/2,-y+1/2,z+1/2
#7 x-1,y,z #8 x-1/2,y-1/2,z .

Table S3. The comparison of the proposed sensor with other reported sensors for ATV determination with application in real samples.

Material	Detection technique	LOD (M)	Real Sample	Ref
AuNP-CNT/SPCE[a]	Electrochemistry	1.9×10^{-7}	Tablet	[1]
Fe_3O_4@PPY / MWCNTs/ GE[b]	Electrochemistry	2.3×10^{-8}	Tablet / human serum	[2]
EPPGE[c]	Electrochemistry	2.1×10^{-5}	Tablet	[3]
PPY/CNTs/GCE[d]	Electrochemistry	1.5×10^{-9}	Tablet	[4]
ZnO/NS/ CPE[e]	Electrochemistry	2.5×10^{-9}	Tablet / urine	[5]
VACNT-GO[f]	Electrochemistry	9.4×10^{-9}	Urine / human serum	[6]
CPE in micelles[g]	Electrochemistry	4.0×10^{-9}	Tablet / urine	[7]
boron-doped diamond electrode	Electrochemistry	2.7×10^{-7}	Tablet / urine	[8]
Ce(IV)-benzothiazolinone hydrazone complex	Spectrophotometry	8.2×10^{-6}	Tablet	[9]
Zn-LMOF	Fluorescence	4.2×10^{-6}	Tablet	This work

[a]AuNP-CNT/SPCE = gold nanoparticles-carbon nanotubes/screen-printed carbon based electrode
[b]Fe_3O_4@PPY / MWCNTs/ GE= graphite electrode modified with polypyrrole-coated Fe_3O_4 nanohybrid by core-shell structure (Fe_3O_4@PPyNPs) and multiwall carbon nanotubes (MWCNTs)
[c]EPPGE = edge-plane pyrolytic graphite electrode
[d]PPY /CNTs / GCE = polypyrrole/carbon nanotube/glassy carbon electrode
[e]ZnO/NS/ CPE = zinc oxide nanoparticles and nano-silica carbon paste electrode
[f]VACNT-GO electrode = vertically aligned carbon nanotube/graphene oxide
[g]CPE = carbon paste electrode

1 R. O. Gunache, A. V. Bounegru and C. Apetrei, *Inventions*, 2021, **6**, 57.
2 A. Tavousi, E. Ahmadi, L. Mohammadi-Behzad, V. Riahifar and F. Maghemi, *Microchem. J.*, 2020, **158**, 105159.
3 O. Fazlolahzadeh, A. Rouhollahi and M. Hadi, *Anal. Bioanal. Electrochem.*, 2016, **8**, 566–577.
4 Z. Kamalzadeh and S. Shahrokhian, *Bioelectrochemistry*, 2014, **98**, 1–10.
5 S. D. Bukkitgar, N. P. Shetti and R. M. Kulkarni, *Sensors Actuators, B Chem.*, 2018, **255**, 1462–1470.
6 T. A. Silva, H. Zanin, F. C. Vicentini, E. J. Corat and O. Fatibello-Filho, *Analyst*, 2014, **139**, 2832–2841.
7 J. C. Abbar and S. T. Nandibewoor, *Colloids Surfaces B Biointerfaces*, 2013, **106**, 158–164.
8 B. Dogan-Topal, B. Uslu and A. S. Ozkan, *Comb. Chem. High Throughput Screen.*, 2007, **10**, 571–582.
9 S. Ashour, M. Bahbouh and M. Khateeb, *Spectrochim. Acta - Part A Mol. Biomol. Spectrosc.*, 2011, **78**, 913–917.

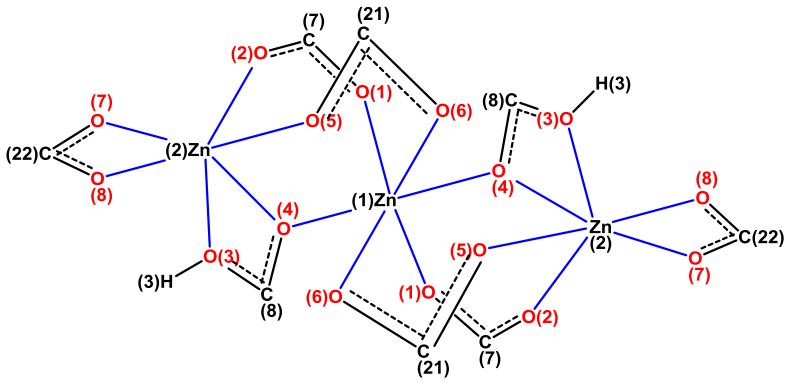

A

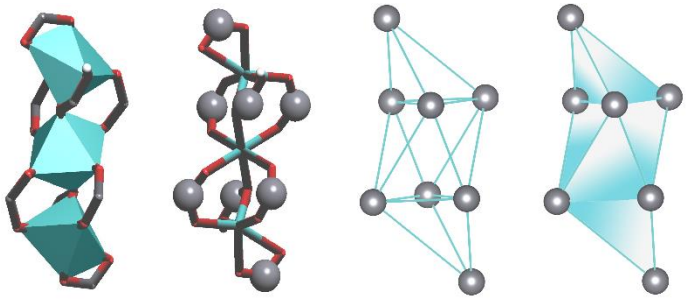

B

Fig. S1. A) Coordination mode of trinuclear SBUs of **1** and B) Schematic illustrations of the trinuclear core.

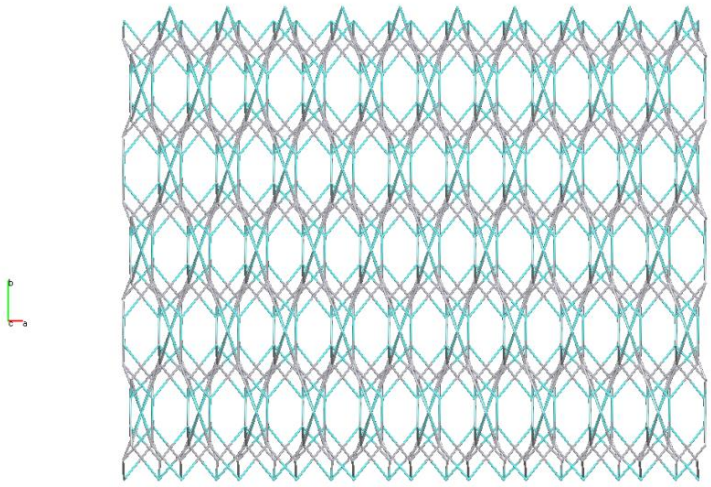

Fig. S2. Simplified topology network of **1**.

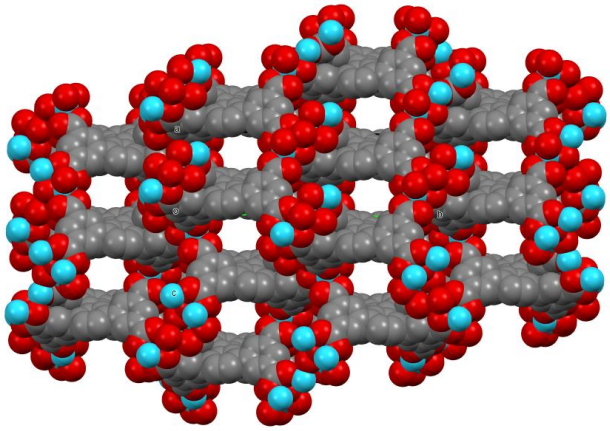

Fig. S3. Space-filling views of **1**, showing pores, view along a plane perpendicular to *ac* plane (hydrogen atoms and lattice molecules are omitted for clarity). Atom codes: Zn (blue), C (grey), O (red) and H (white).

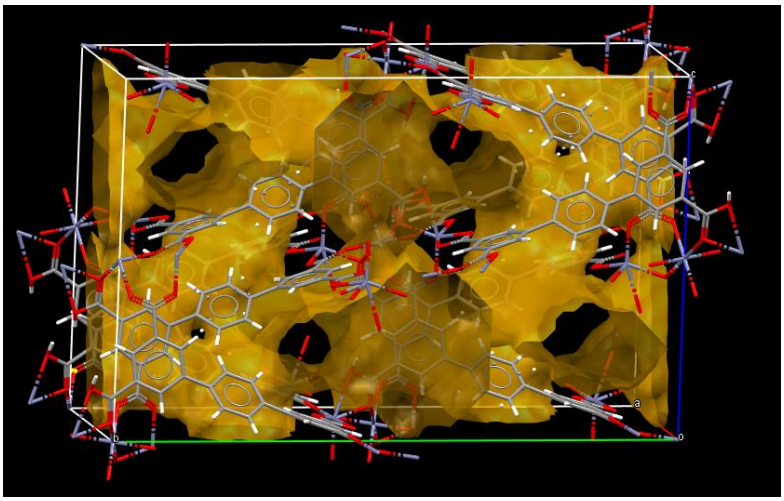

Fig. S4. Void surfaces for a packing section of **1**; view along *a* axis. Zn (blue), C (grey), O (red) and H (white).

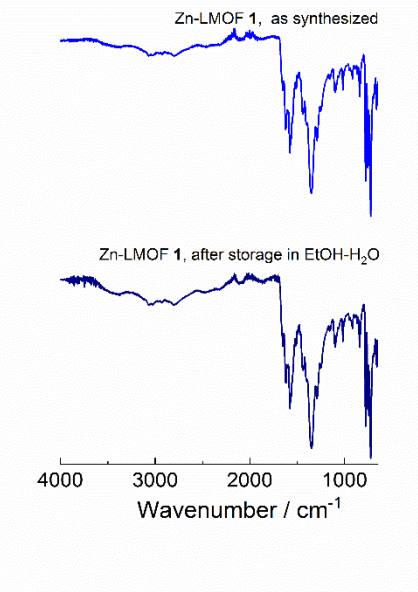

Fig. S5. IR spectra of Zn LMOF **1** before and after storage in ethanol-water for 24 hours.

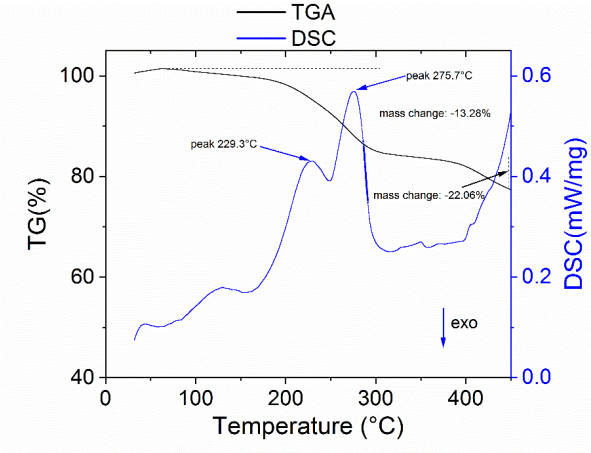

Fig. S6. TGA curve and DSC of Zn-LMOF **1**.

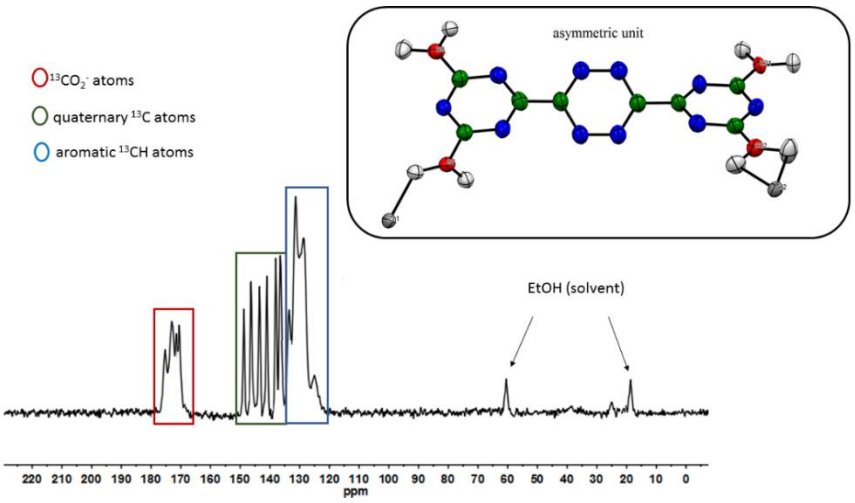

Fig. S7. ^{13}C ss-CPMAS NMR (spinning rate at 8 kHz) spectrum for **1** and the asymmetric unit from the crystal structure (above).

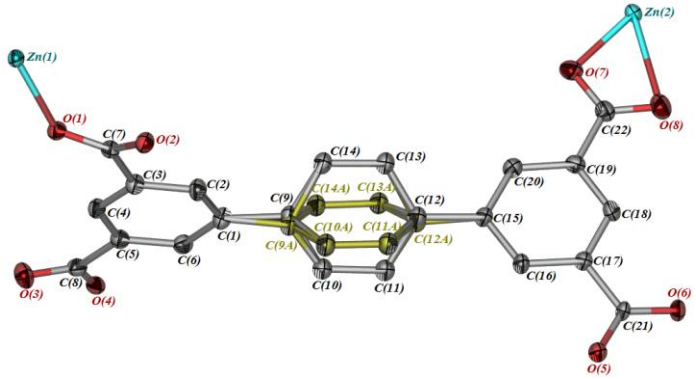

Fig. S8. Rotational disorder of central phenyl in the crystal of **1**.

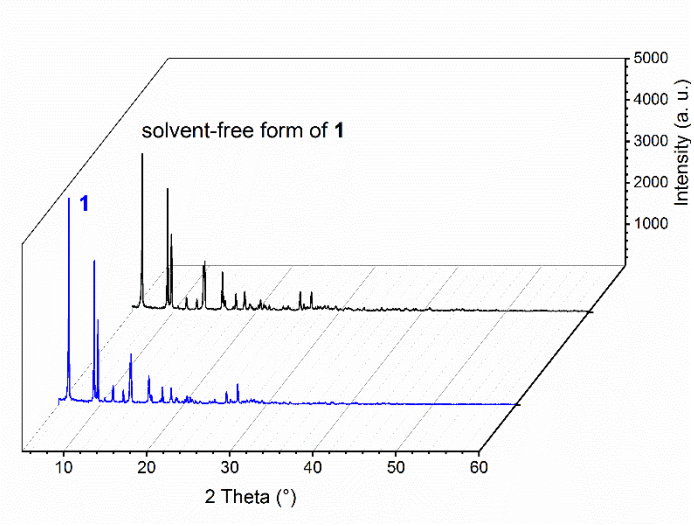

Fig. S9. PXRD patterns of **1** and its solvent-free form.

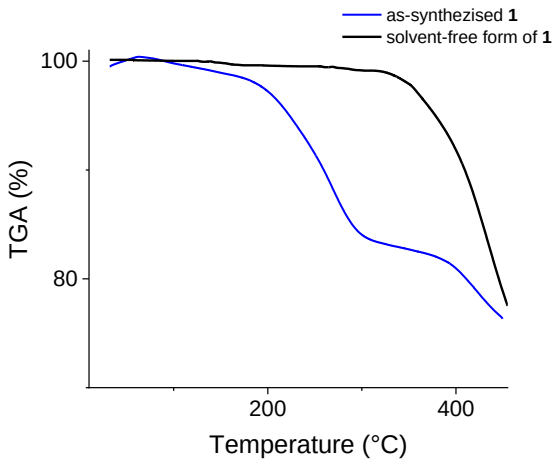

Fig. S10. TGA curves of **1** and its solvent-free form.

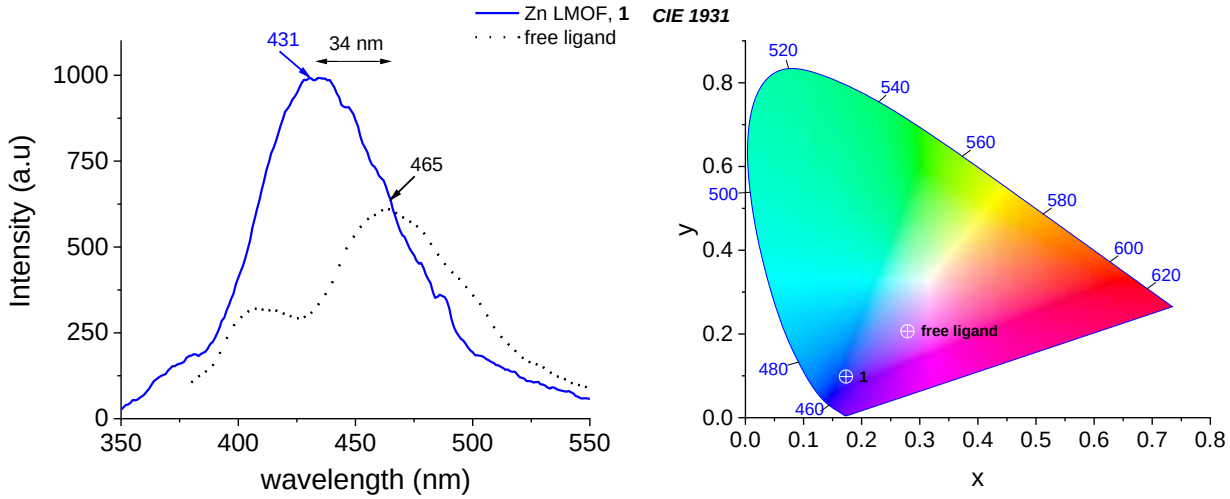

A B

Fig. S11. A) Solid-state emission spectra of Zn- MOF **1** (solid line) and free H_4tptc ligand (dot line). B) CIE-1931 chromaticity diagram of **1** and free H_4tptc ligand.

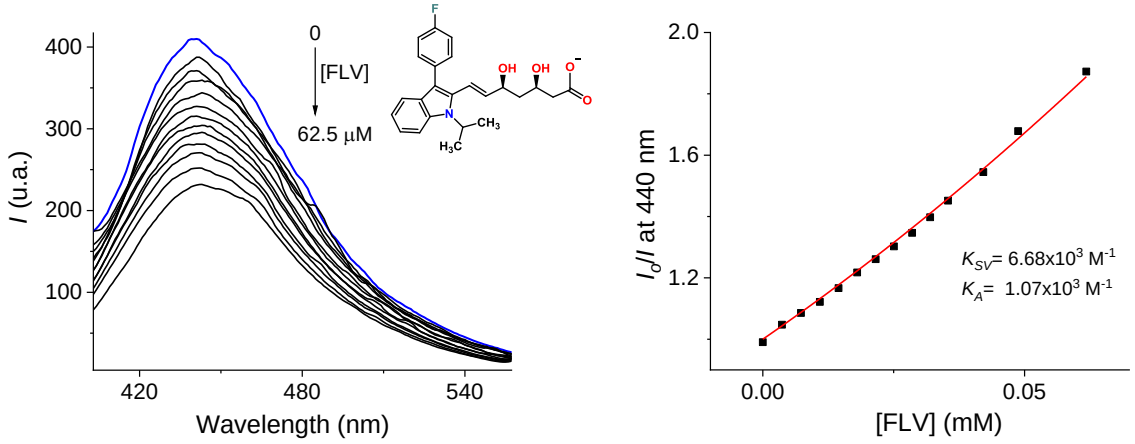

A B

Fig. S12. A) Emission spectra (λ_{ex}= 330 nm) of **1** dispersed in ethanol-water (8/2, v/v) at pH= 7.0 upon additions of increasing amounts of FLV sodium. B) Stern-Volmer plot at 440 nm, the solid line was obtained by fitting to Eq. (2).

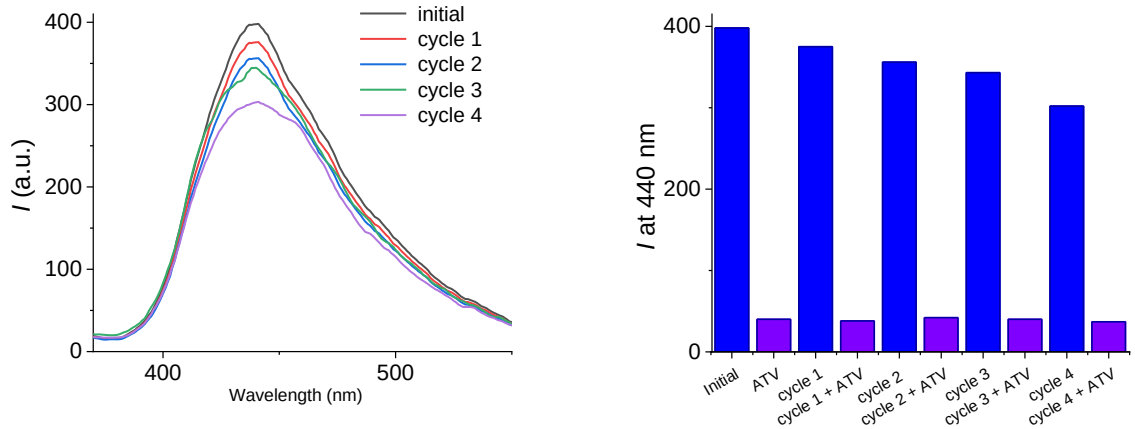

A B

Fig. S13. A) Photoluminescence spectra of **1** after four cycles of ATV detecting-removal in ethanol-water at pH= 7.0. B) Quenching efficiencies of 1 in four cycles of ATV detection, in which **1** was treated with ethanol-DMF for the next cycles of detection.

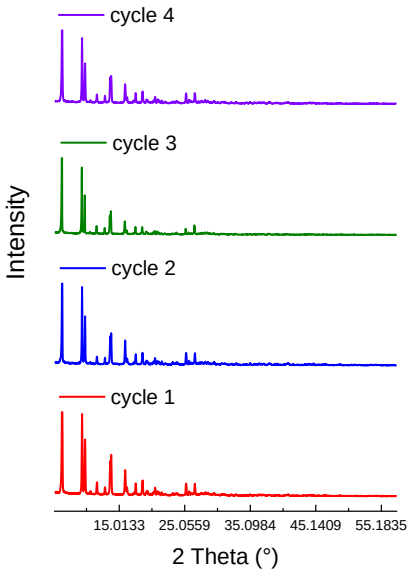

Fig. S14. PXRD pattern of **1** after four cycles of ATV detecting-removal.

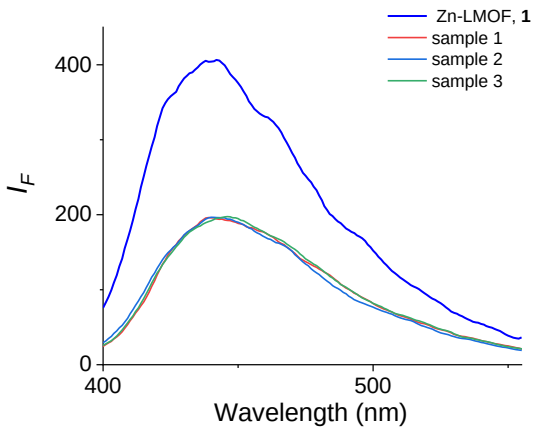

Fig. S15. Emission spectra (λ_{ex}= 330 nm) of **1** dispersed in ethanol-water (8/2, v/v) at pH= 7.0 upon additions of ATV from real pharmaceutical samples (Eturium 20). The test was carried out in triplicate.

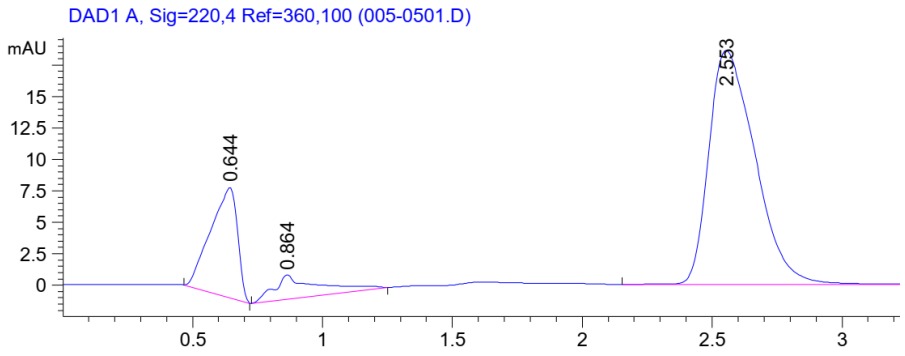

A

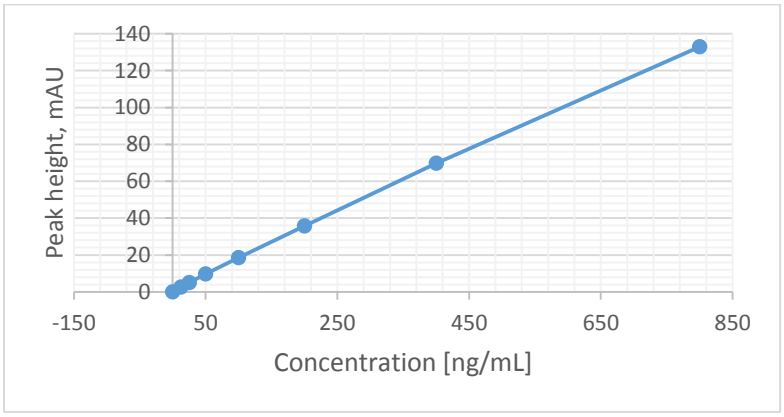

B

Fig. S16. A) HPLC chromatogram of pure standard of atorvastatin calcium [100 ng/mL]. B) Calibration curve showing the peak height (mAU) as a function of atorvastatin calcium concentration [ng/mL]. The corresponding peak for atorvastatin is 2.55 min.

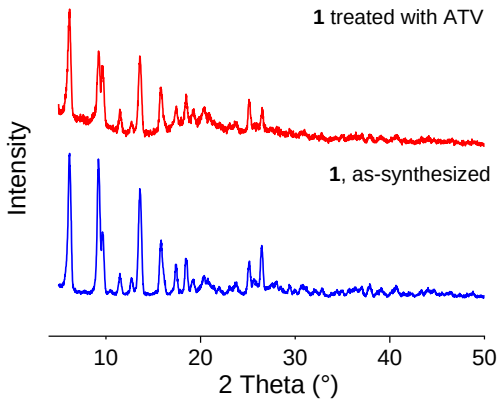

Fig. S17. PXRD pattern of as-synthesized **1** and **1** treated with ATV calcium for 24 h.

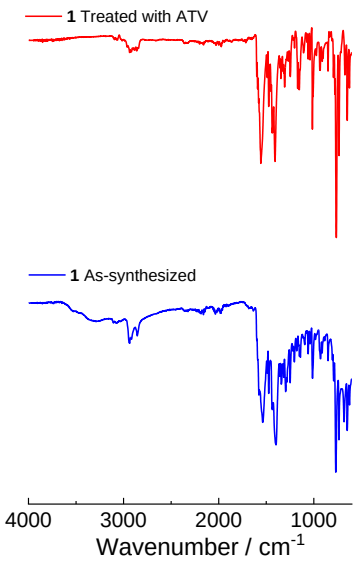

Fig. S18. IR spectra of as-synthesized **1** and **1** treated with ATV calcium for 24 h.

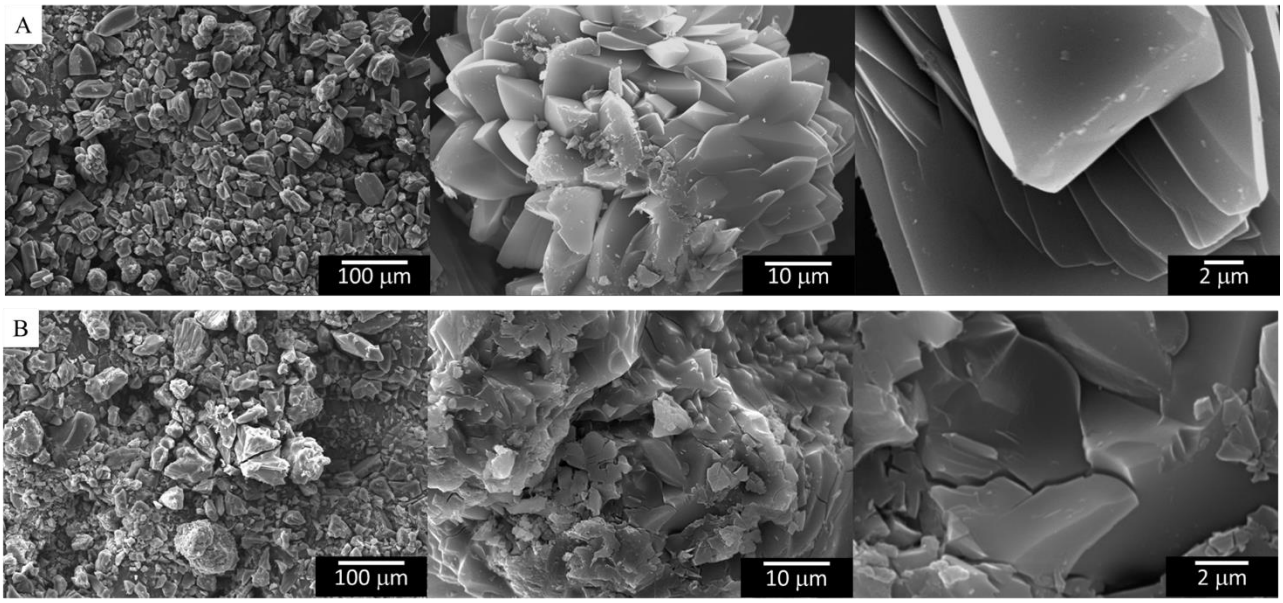

Fig. S19. SEM micrographs collected at different magnifications of A) as-synthesized **1** and b) **1** treated with ATV calcium.

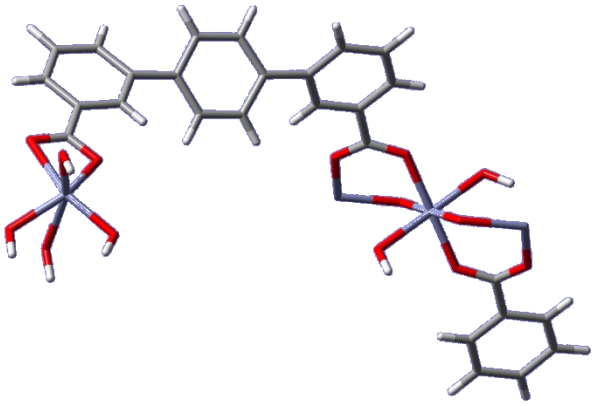

Fig. S20. A selected representative section of **1** to calculate interaction with ATV.